Applied Surface Science 580 (2022) 152167

Contents lists available at ScienceDirect

Applied Surface Science

journal homepage: www.elsevier.com/locate/apsusc

Full Length Article

Efficiency of exciton splitting in organic photovoltaic cells within EQE spectrum

Grażyna Jarosz *, Rafał Marczyński, Ryszard Signerski

Institute of Physics and Computer Science, Faculty of Applied Physics and Mathematics, Gdansk University of Technology, 80-233 Gdansk, Poland

ARTICLE INFO

Keywords:
Organic photovoltaics
Electron donor-electron acceptor junction
Exciton diffusion
Exciton splitting
Excitonic photovoltaic cell

ABSTRACT

The paper presents a procedure of estimating the efficiency of exciton splitting at ED/EA interface. The procedure consists in evaluation of splitting of excitons into electron-hole pairs on the basis of the external quantum efficiency spectra of planar cells and spectra of absorbance of active organic layers. The fitting parameters are the exciton splitting probabilities at ED/EA interface. The presented procedure was applied to two different photovoltaic systems: ITO/MoO_3/DBP/PTCBI/BCP/Ag and ITO/MoO_3/DBP/F_{16}ZnPc/BCP/Ag with quite similar energy diagrams at the ED/EA interface. The analysis performed led us to the conclusion that only the DBP/PTCBI interface can be considered attractive for organic photovoltaics and organic photodetection, while the DBP/F_{16}ZnPc interface does not show any favourable properties for such applications.

1. Introduction

Three to five percent less, the limit of power conversion efficiency of single-junction organic photovoltaic cells is estimated lower than that of single-junction semiconductor cells [1–6]. These three to five percent are related to the need to create appropriate conditions for the dissociation of an exciton to electron-hole pair [2,6–9]. Davydov-Frenkel excitons, which are generated in organic materials, are tightly bound and do not dissociate spontaneously into electron-hole pairs [2,6–8,10]. However, with an appropriate offset at the electron donor (ED)/electron acceptor (EA) interface, the exciton reaching this interface can transform into charge-transfer (CT) pair with an electron on the EA molecule and a hole on the ED molecule [1,5,11–13]. If this CT state successfully dissociates, we get an electron that penetrates EA and a hole that penetrates ED. If the ED and EA layers are equipped with properly selected electrodes, that is, the hole-collecting electrode (HCE) on the ED layer and the electron-collecting electrode (ECE) on the EA layer, it can be said that there are suitable conditions for generating the photovoltaic current in the device. This current is created by electrons moving in EA from ED/EA junction to ECE and holes moving in ED from ED / EA junction to HCE.

The appropriate set of energy levels is obtained for materials whose transport levels provide the sufficient energy gap between the electron-transporting level (ETL) in EA and the hole-transporting level (HTL) in ED. Simultaneously, the HTL in the EA should be below the HTL in the ED, and the ETL in ED should be above the ETL in the EA. Such an energy diagram is necessary to generate photovoltaic current in excitonic cells, because then the excitons reaching the ED/EA interface may spontaneously dissociate into the appropriate CT states [2,3,6,14–16]. In organic layers the ETL and HTL are often named as LUMO and HOMO, respectively. However, it is worth emphesizing that energies of electron levels in organic layers are not equal to energies of electron states in single molecules. The problem of splitting an exciton into free charge carriers is currently quite widely discussed in the literature, e.g. [14–18]. Experimental studies show, however, that the presence of an appropriate energy structure at the ED/EA junction does not guarantee an efficient photovoltaic process. The splitting of the excitons reaching the ED/EA junction into free carriers is obviously determined by exciton kinetics occurring at ED/EA interfaces. Important stage in this process is generation of CT states with the electron on the molecule of EA and the hole on the molecule of ED. Additionaly, the splitting of excitons at the ED/EA junction can be suppressed by additional surface quantum states at the interface. These states can quench excitons directly or by trapping them earlier, they can also trap charge carriers at the interface and thus create unfavourable recombination centres [6, 8, 14, and 19]. So in general, the appropriate energy relation of the transport levels in ED and EA is a necessary but not sufficient condition to assess the possibility of using a specific ED/EA junction in a photovoltaic system.

Research on organic photovoltaic cells is currently conducted mainly on bulk structures, usually denoted as ED:EA. In such structures, the ED/

* Corresponding author.
E-mail address: grajaros@pg.edu.pl (G. Jarosz).

https://doi.org/10.1016/j.apsusc.2021.152167
Received 1 November 2021; Received in revised form 29 November 2021; Accepted 7 December 2021
Available online 17 December 2021

EA interface is highly developed and very irregular. This research direction is dictated by a too short exciton diffusion length in relation to the layer thickness necessary for adequate absorbance of incident radiation [19–22]. In bulk structures, theoretically, all excitons generated in active layers can reach the ED/EA interface during their lifetime. However, assessment of the effectiveness of splitting an exciton into an electron-hole pair becomes quite difficult. Therefore, before moving on to the tedious optimization of a system, it is worth using a tool that would allow an experimentally assessment of the effectiveness of splitting excitons in structures with an ED/EA junction.

In this work, we suggest an evaluation of splitting of excitons into electron-hole pairs on the basis of the external quantum efficiency spectra (*EQE*) of planar cells and spectra of absorbance of active layers. As we will show, in planar systems it is easy to separate *EQE* into individual processes, which in turn lead from the absorption of photons to the generation of a short-circuit current. We will use the presented approach to evaluate two junctions with quite similar ED/EA energy diagrams.

In the systems under study the role of ED was played by DBP (tetraphenyldibenzoperiflanthene) layer. This is a material of high values of VIS absorption coefficient and relatively high value of exciton diffusion length in vacuum deposited layers [23–28]. F_{16}ZnPc (perfluorinated zinc phthalocyanine) [29] and PTCBI (perylenetetracarboxylic bisbenzimidazole) [7,30] were used as EA material. Both materials have a wider absorption band than DBP and an energy diagrams suitable for efficient exciton dissociation at the ED/EA interface can be seen for both the junctions with DBP, namely for DBP/F_{16}ZnPc and for DBP/PTCBI. Moreover, both the junctions could be an alternative for fullerene solar cells, that are of poor thermal and air stability [31,32].

2. Theoretical backgroud

In organic photovoltaic cells, as for semiconductor cells, the generation of electron-hole pair is usually a one-photon process. It means that one photon can generate no more than one electron-hole pair. The definition of external quantum efficiency takes the form:

$$EQE = \frac{J_{sc}}{eI_o} \tag{1}$$

where e– elementary charge, I_o– surface density of photon flux incident on a cell, J_{sc} – density of short-circuit current.

Taking into account the subsequent steps leading to the formation of the electron-hole pair in excitonic cells, the *EQE* value can be presented as the following product:

$$EQE = \eta_{transition} \times \eta_{ph-ex} \times \eta_{G_{ex}-\phi_{ex}} \times \eta_{splitting} \tag{2}$$

where $\eta_{transition}$ – effective transmittance coefficient of all the layers that must be penetrated by radiation before reaching active organic layer, η_{ph-ex} –exciton generation efficiency, $\eta_{G_{ex}-\phi_{ex}}$ – probability that the exciton will reach the ED/EA interface, $\eta_{splitting}$ – probability that the exciton reaching the ED/EA interface will split into an electron-hole pair.

The coefficient $\eta_{transition}$ is defined as the ratio of flux density of photons reaching the organic active layer 1 (I_{o1}) to flux density of photons incident on the cell (I_o). This will then be determined by transmittance of the radiation across successive interfaces, namely air-electrode, electrode-buffer layer, buffer layer-organic active layer. In addition, the absorption of radiation in both outer layers, the buffer and the outer electrode, can also reduce value of this coefficient. In the case when outer electrode is deposited on a transparent substrate, the substrate also affects the $\eta_{transition}$ value.

The coefficient η_{ph-ex} is defined as the ratio of the amount of excitons generated per unit time interval in organic layers per unit area of the cell to the photon flux density entering the outer active organic layer. It expresses the probability that a photon entering active layers will generate an exciton. In the exciton bands, absorption of a photon leads to generation of an exciton. If there is no other types of absorption, the coefficient η_{ph-ex} can be directly derived from the absorbance (*ABS*) of the organic layers:

$$\eta_{ph-ex} = 1 - 10^{-(ABS_1+ABS_2)} \tag{3}$$

where ABS_1 and ABS_2 are absorbance of the layer 1 and the layer 2, respectively. Thereafter, the layer which the light penetrates first will be denoted by subscript 1. The layer 2 is the layer into which the radiation penetrates after passing through layer 1. The structure of the sample and the reference x-axis is shown in Fig. 1.

The $\eta_{G_{ex}-\phi_{ex}}$ factor is defined as the ratio of the exciton flux density reaching the ED/EA interface to the amount of excitons generated per unit time interval in active organic layers per unit area of the cell. This coefficient can be presented in the form:

$$\eta_{G_{ex}-\phi_{ex}} = \frac{\phi_1 + |\phi_2|}{I_{o1}(1 - 10^{-(ABS_1+ABS_2)})} \tag{4}$$

where ϕ_1 and ϕ_2 are the densities of exciton flux reaching the ED/EA interface from the side of the layer 1 and from the side of the layer 2, respectively. Fluxes of ϕ_1 and ϕ_2 are determined by the distribution of excitons in organic layers, and this distribution depends on exciton generation rate distribution, exciton lifetime (τ) and the exciton diffusion length (L) as well as on the interaction of excitons with the surfaces of the layers. In excitonic photovoltaic cells, the advantageous situation is that the excitons reaching the electrodes are fully reflected, which should be provided by selected buffer layers. On the other hand, excitons reaching the ED/EA interface should encounter an appropriate set of energy levels that will allow the efficient splitting of the excitons into electron-hole pairs. However, even when exciton splitting does not occur with high efficiency, the presence of quantum states with energy lower than the exciton energy usually leads to effective quenching of excitons. Therefore, it can be assumed that excitons reaching the ED/EA interface are completely quenched. Due to the solution of exciton

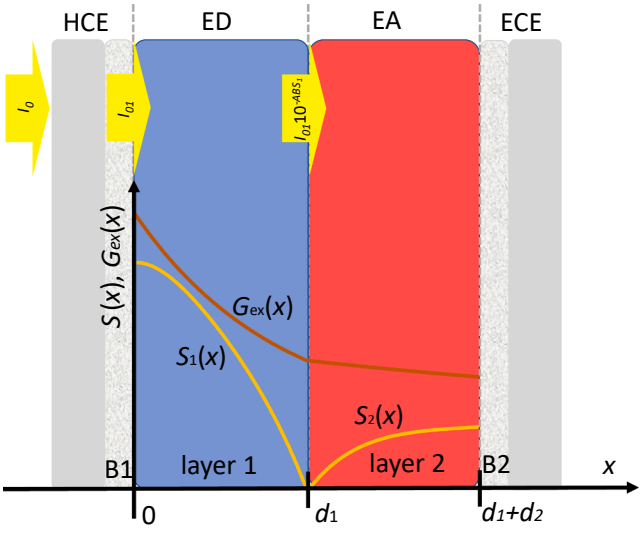

Fig.1. Structure of a planar organic photovoltaic cell, assuming that the outer active organic layer (layer 1) is made of ED material and the inner active layer (layer 2) is made of EA material. The active layer are provided with buffer layers, namely layer 1 with the buffer layer B1 and layer 2 with the buffer layer B2. The thickness of layer 1 is d_1 and the thickness of layer 2 is d_2. The origin of x-axis is located at the B_1/layer 1 interface. The vertical axis presents both concentration of excitons in arbitrary unit and exciton generation rate in arbitrary unit. Brown line schematically shows the distribution of exciton generation rate, i.e. the first term on the left in (5), and yellow line shows the exciton distribution in active layers of the cell, i.e. the solution of (5) under the boundary conditions (6) and (7).

diffusion equation:

$$\kappa_i I_{oi}\exp(-\kappa_i x) - \frac{1}{\tau_i}S_i(x) - D_i\frac{d^2S_i(x)}{dx^2} = 0 \tag{5}$$

under the following boundary conditions for layer 1

$$\left.\frac{dS_1(x)}{dx}\right|_{x=0} = 0 \quad and \quad S_1(d_1) = 0 \tag{6}$$

and for layer 2

$$S_2(d_1) = 0 \quad and \quad \left.\frac{dS_2(x)}{dx}\right|_{x=d_1+d_2} = 0 \tag{7}$$

we can find the formula for ϕ_1 i ϕ_2 from:

$$\phi_1 = -D_1\left.\frac{dS_1(x)}{dx}\right|_{x\to d_1^-} \tag{8}$$

$$\phi_2 = -D_2\left.\frac{dS_2(x)}{dx}\right|_{x\to d_1^+} \tag{9}$$

where $i = 1$ refers to layer 1 and $i = 2$ to layer 2, $S_1(x)$ and $S_2(x)$ are exciton concentrations in the layers, κ_1 and κ_2 are the linear absorption coefficients, d_1 and d_2 are layer thicknesses, τ_1 and τ_2 are exciton lifetimes in the layers, D_1 and D_2 are diffusion coefficients defined as $D_1 = L_1^2/\tau_1$ i $D_2 = L_2^2/\tau_2$. The value I_{oi} expresses the flux density of photons entering the i-th layer. Neglecting reflection of light at ED/EA interface we can take $I_{o2} = I_{o1}\exp(-\kappa_1 d_1)$.

In discussion on exciton kinetics at ED/EA interface the Q parameter is taken into consideration [14,16]. This parameter characterizes the surface quenching of excitons generated in the i-th layer and it is defined as:

$$Q_i = 1 - \frac{S_{iwithED/EA}}{S_{iwithoutED/EA}} \tag{10}$$

where $S_{iwithED/EA}$ is the concentration of singlet excitons in the i-layer near the ED/EA interface and $S_{iwithoutED/EA}$ is the concentration of singlet excitons in the i-layer in the absence of the second layer.

The value of Q_i approaching 1 means that excitons are effectively quenched by the interface, so the sum of recombination and splitting rates of singlet excitons near the interface is much greater than in the bulk of the i-layer. In the case of $Q_i = 0$, the recombination and splitting rates of singlet excitons near the ED/EA interface are of the same value as in the bulk of the i-layer. Translating Q_i to the boundary conditions for the exciton diffusion equation, (6) and (7), one can notice that $Q_i = 1$ refers to the conditions $S_1(d_1) = 0$ and $S_2(d_1) = 0$, while $Q_i = 0$ refers to the conditions $\left.\frac{dS_1(x)}{dx}\right|_{x=0} = 0$ and $\left.\frac{dS_2(x)}{dx}\right|_{x=d_1+d_2} = 0$.

The flux of excitons reaching the ED/EA interface, calculated according to (8) and (9) from the solution of equation (5) under boundary conditions (6) and (7), takes the following forms:

- for excitons reaching the ED/EA interface from the layer 1:

$$\phi_1 = \frac{(L_1\kappa_1)I_{o1}}{(1-(L_1\kappa_1)^2)}\left(L_1\kappa_1 e^{-\kappa_1 d_1} - \frac{A_1 e^{\frac{d_1}{L_1}} + B_1 e^{-\frac{d_1}{L_1}}}{C_1}\right) \tag{11}$$

with $A_1 = L_1\kappa_1 e^{-\frac{d_1}{L_1}} - e^{-\kappa_1 d_1}$

$B_1 = L_1\kappa_1 e^{\frac{d_1}{L_1}} + e^{-\kappa_1 d_1}$

$C_1 = e^{-\frac{d_1}{L_1}} + e^{\frac{d_1}{L_1}}$

- for exciton reaching the ED/EA interface from the layer 2:

$$\phi_2 = \frac{(L_2\kappa_2)I_{o1}10^{-ABS_1}}{(1-(L_2\kappa_2)^2)}\left(\kappa_2 L_2 - \frac{A_2 + B_2}{C_2}\right) \tag{12}$$

with $A_2 = L_2\kappa_2 e^{-\kappa_2 d_2} - e^{-\frac{d_2}{L_2}}$

$B_2 = L_2\kappa_2 e^{-\kappa_2 d_2} + e^{\frac{d_2}{L_2}}$

$C_2 = e^{\frac{d_2}{L_2}} + e^{-\frac{d_2}{L_2}}$

Since the flux ϕ_2 is directed opposite to the x-axis, the absolute value of ϕ_2 is inserted into (4).

The fluxes of ϕ_1 and ϕ_2 depend on the following products: $L_i\kappa_i$, $\kappa_i d_i$, and the ratio d_i/L_i, however does not depend on τ_i. It can be said that only indirectly the fluxes of ϕ_1 and ϕ_2 depend on τ_i, because for long-lived excitons, e.g. for triplet excitons, L_i can be explicitly higher. However, the fluxes of ϕ_1 and ϕ_2 are determined directly by L_i. At this point it is worth adding that excitons usually generated in organic cells are singlet excitons with the lifetime equal to 10^{-8} s.

Quenching of excitons at the ED/EA interface can occur in several ways. For example, excitons that reach the ED/EA interface can become trapped and then spontaneously recombine. They can also be quenched by charge carriers trapped at the ED/EA interface. Finally, with appropriate energy offset, they can dissociate to CT states with electrons on EA molecules and holes on ED molecules. If bounding energy of such a state is not too high, the charge carriers of the pairs can start to penetrate organic layers, while electrons penetrate EA layer and holes penetrate ED layer [2]. It is worth emphasizing here that $Q_i \to 1$ at $x = d_1$ always indicates strong quenching at the ED/EA interface but does not necessary imply effective generation of electron-hole pair. However, the occurance of J_{sc} in the system with ED/EA simultaneously with an adequete correlation between spectra of J_{sc} and exciton absorption always results from exciton dissociation at ED/EA interface.

If ECE and HCE are short-circuited, the current flowing in the cell is determined by the generation rate of electron-hole pairs. By assigning the probability that an exciton reaching ED/EA interface dissociates to the CT state by P_{Si}, the efficiency of exciton splitting can be represented as:

$$\eta_{splitting} = \frac{P_{S1}\phi_1 + P_{S2}|\phi_2|}{\phi_1 + |\phi_2|} \tag{13}$$

where P_{S1} i P_{S2} are probabilities of CT generation at the ED/EA interface by exciton reaching the interface, from layer 1 and layer 2, respectively.

The P_{Si} value of 1 can only be achieved when each exciton that reaches the interface generates an electron-hole pair. This happens when other processes leading to exciton quenching at the ED/EA interface are negligible. Such an ED/EA interface would be considered ideal and values of P_{Si} close to 1 should be regarded as worth of further development in both planar and bulk photovoltaic structures. The high value of $\eta_{splitting}$ can be considered attractive for photovoltaics and for detection of VIS radiation [7].

3. Details of procedure

According to (1) the spectrum of *EQE* can be derived from the J_{sc} spectrum measured with a constant flux of incident photons. Apar from $\eta_{splitting}$, the *EQE* is determined by three factors, namely η_{ph-ex} , $\eta_{G_{ex}-\phi_{ex}}$ and $\eta_{transition}$. The first one, i.e. η_{ph-ex}, is easy to estimate, because according to (3) it can be obtained from absorbance spectra of active layers. It can be also obtained from spectra of linear absorption coefficient of the active layers and their thickness. The second factor, i.e. $\eta_{G_{ex}-\phi_{ex}}$ defined by (4), can be estimated using (11) and (12). The exciton diffusion lengths in ED and EA layers are also needed here. There are many methods of determining exciton diffusion length in organic layers,

and the values of this parameter are well defined for many organic materials [19]. We can then use literature data.

Quite a complex issue is the factor $\eta_{transition}$. As mentioned above, its spectrum results from all the transmission and absorption processes that the photon flux undergoes before reaching the layer 1. We suggest to solve this problem experimentally, namely by measuring J_{sc} at a constant value of the photon flux density entering the layer 1. In this case, we do not control the flux of photons incident on the device, but the photon flux that has passed through the glass substrate, outer electrode and the buffer layer B1. We assumed that it corresponds to the value of I_{o1}. Due to definition of EQE (Eq. (1)) and definition of $\eta_{transition}$, we find the following relationships:

$$\frac{J_{sc}}{eI_{o1}} = \frac{EQE}{\eta_{transition}} \tag{14}$$

The J_{sc} measurements made in the above manner result in an experimental spectrum of $EQE/\eta_{transition}$. The product of $\eta_{ph-ex} \times \eta_{G_{ex}-\phi_{ex}} \times \eta_{splitting}$ can be compared with this spectrum. As described above, $\eta_{ph-ex} \times \eta_{G_{ex}\to\phi_{ex}}$ depends on the thickness of organic layers, their linear absorption coefficients and the values of exciton diffusion length in both layers. Only $\eta_{splitting}$ is an unknown factor, which due to the dependence on ϕ_1 and ϕ_2, is also a function of wavelength. The spectrum of $\eta_{splitting}$ is shaped by the probability of splitting the exciton into an electron-hole pair. It is obvious that this probability may have different values for different excitons, i.e. for excitons reaching the ED/EA interface from different layers. Therefore , the exciton-splitting probability for the layer 1 is noted as P_{S1} and for the layer 2 is noted as P_{S2}. To correlate $\eta_{ph-ex} \times \eta_{G_{ex}-\phi_{ex}} \times \eta_{splitting}$ with $EQE/\eta_{transition}$ we can change P_{S1} and P_{S2} within the range [0,1].

4. Application

The procedure outlined above was used to estimate the efficiency of exciton dissociation at two different ED/EA interfaces. Structural formulae of molecules used as ED and EA are shown in Fig. 2. Both EA materials, namely F_{16}ZnPc and PTCBI, have a wider absorption band than DBP used as ED material but the maximum values of the linear absorption coefficient are lower than that of DBP. The absorption spectrum of F_{16}ZnPc is shifted with respect to DBP towards the longer wavelengths and the PTCBI absorption spectrum covers the whole band of strong DBP absorption. However, as was mentioned in *Introduction* the energy diagrams of DBP/F_{16}ZnPc and DBP/PTCBI are quite similar and seem to be suitable for efficient exciton dissociation at the ED/EA interface. The diagrams of energy levels are depicted in Fig. 2. The difference between the electron-transporting level in EA and the hole-transporting level in ED can be estimated at 0.9 eV for DBP/F_{16}ZnPc [24,33], and at 1.0 eV [24,30,34] or 1.5 e V [24,35] for DBP/PTCBI.

In our devices, the ITO/MoO_3 (indium tin oxide/molybdenum trioxide) double layer was applied as HCE and the BCP/Ag (bathocuproine/Ag) double layer was applied as ECE. The MoO_3 buffer layer was incorporated into the system to facilitate hole extraction from DBP to ITO, as well as to reduce exciton quenching at ITO [26,29,36,37], while BCP was used to improve electron collection at Ag electrode, and to prevent damage of the EA layer caused by penetration of Ag atoms upon the electrode deposition [26,27]. The analyzed systems have the following structures: MoO_3(5)/DBP(17)/F_{16}ZnPc(65)/BCP(15)/Ag(50) and MoO_3(5)/DBP(38)/PTCBI(60)/BCP(15)/Ag(60). Layer thicknesses are expressed in nm and shown in parentheses. The structures of the samples and the directions of incident radiation are shown in Fig. 2. The sample preparation procedure was described in our previous works [38] and [39].

Figs. 3-7 show the experimental results and their analysis. The J_{sc}

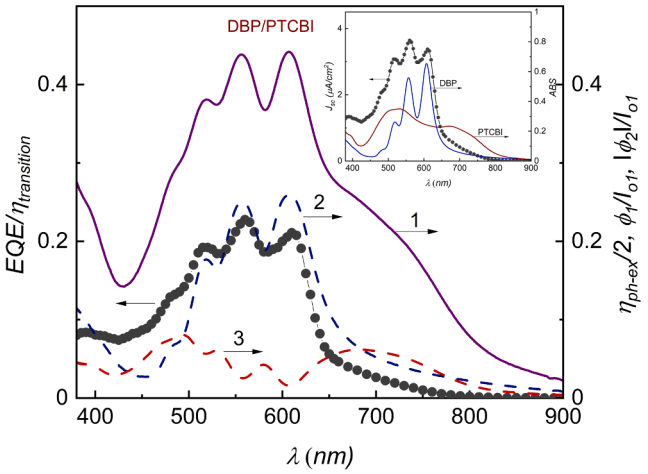

Fig. 3. Spectrum of $EQE/\eta_{transition}$ (circles), spectrum of η_{ph-ex} (line 1), spectrum of ϕ_1/I_{o1} at$L_1 = 16$ nm (line 2) and spectrum of $|\phi_2|/I_{o1}$ at$L_2 = 9$ nm (line 3) are shown in the main body of the figure. The J_{sc} spectrum of the MoO_3/DBP/PTCBI/BCP/Ag system (circles) and *ABS* spectra of the active layers (lines) are presented in the inset. The curves in the main body of the figure were simulated on the basis of experimental results presented in the inset.

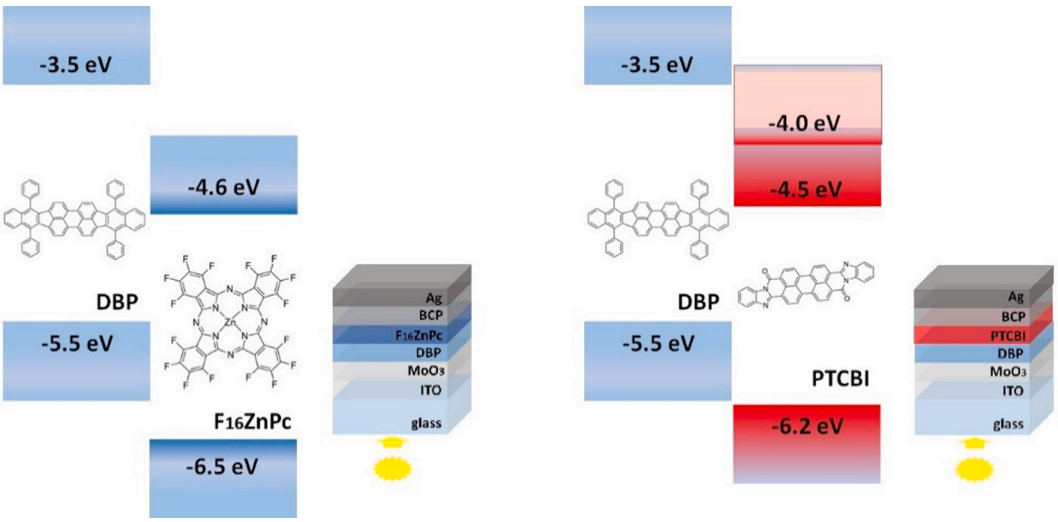

Fig.2. Energy diagrams of investigated organic junction, structural formulae of molecules of active layers and layer structures of investigated devices.

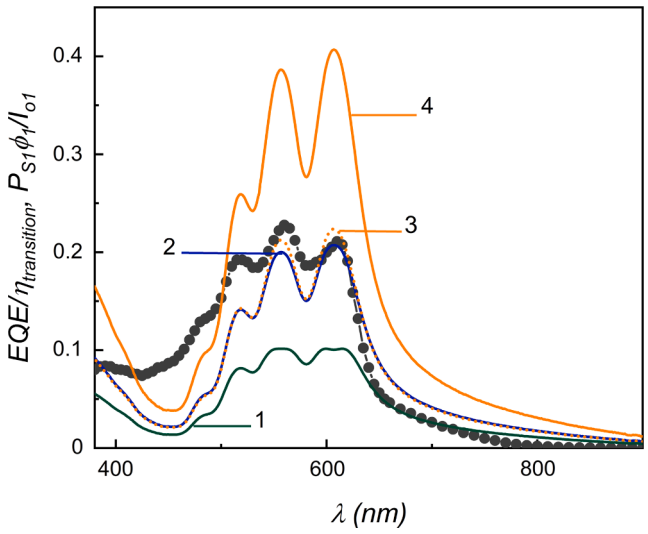

Fig. 4. Spectrum of $EQE/\eta_{transition}$ (circles) and spectra of $P_{S1}\phi_1/I_{o1}$ (lines) for four sets of parameters: 1 -L_1 = 8 nm andP_{S1} = 1; 2 - L_1=16 nm andP_{S1} = 0.8; 3 - L_1=24 nm andP_{S1} = 0.55; 4 - L_1=24 nm andP_{S1} = 1.0. The curves in the figure were simulated on the basis of experimental results presented in the inset of Fig. 3.

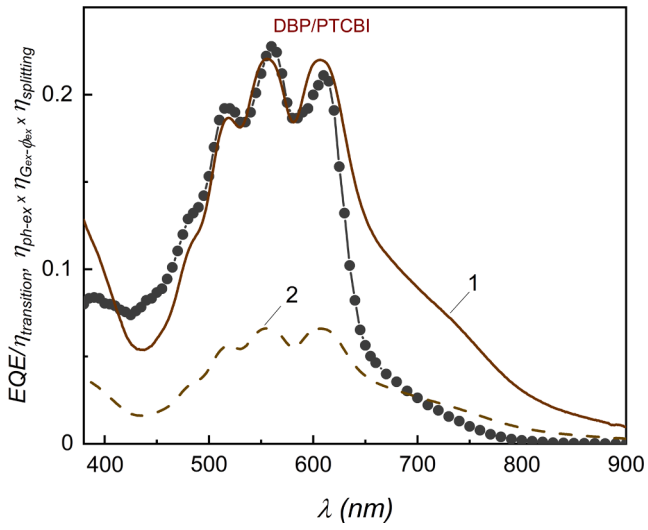

Fig. 5. Spectrum of $EQE/\eta_{transition}$ (circles) and spectra of $\eta_{ph-ex} \times \eta_{G_{ex}-\phi_{ex}} \times \eta_{splitting}$ atL_1 = 16 nm andL_2 = 9 nm for two sets of splitting probability, namelyP_{S1} = P_{S2} = 0.8 (line 1) andP_{S1} = P_{S2} = 0.24 (line 2). The curves were simulated on the basis of experimental results presented in the inset of Fig. 3.

spectra obtained with $I_{o1} = 10^{14}$ photons/(cm^{2}s) and the $EQE/\eta_{transition}$ spectra calculated from J_{sc} according to (14) are presented in the form of solid circles in all figures. The lines in these figures show the *ABS* spectra of the ED and EA layers, as well as ones obtained on their basis: exciton generation efficiency spectra (η_{ph-ex}), spectra of the exciton flux reaching the ED/EA interface divided by I_{o1} (i. e. ϕ_1/I_{o1}, $|\phi_2|/I_{o1}$), and the spectra of the product $\eta_{ph-ex} \times \eta_{G_{ex}-\phi_{ex}} \times \eta_{splitting}$ calculated at particular values of P_{S1} and P_{S2}.

The experimental spectra of J_{sc} and *ABS* of active layers in the tested devices are shown in insets of Fig. 3 and Fig. 6. In the remaining figures solid circles represent the $EQE/\eta_{transition}$ obtained from J_{sc}. Comparing Fig. 3 and Fig. 6, we notice that the maximum of $EQE/\eta_{transition}$ for DBP/PTCBI is almost 5 times greater than for DBP/F_{16}ZnPc. On the other hand, it is seen that the amount of excitons generated per unit time interval is roughly the same, as the maximum value of η_{ph-ex} for the device

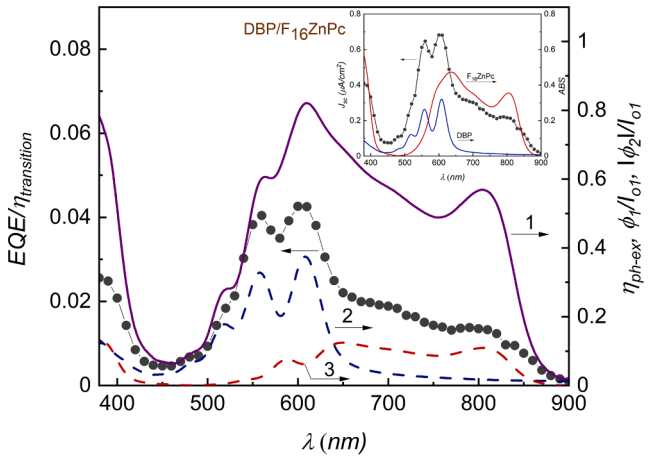

Fig. 6. Spectrum of $EQE/\eta_{transition}$ (circles), spectrum of η_{ph-ex} (line 1), spectrum of ϕ_1/I_{o1} atL_1 = 16 nm (line 2) and spectrum of $|\phi_2|/I_{o1}$ atL_2 = 10 nm (line 3) are shown in the main body of the figure. The J_{sc} spectrum of MoO_3/DBP/F_{16}ZnPc/BCP/Ag system (circles) and *ABS* spectra of the active layers (lines) are presented in the inset. The curves in the main body of the figure were simulated on the basis of experimental results presented in the inset.

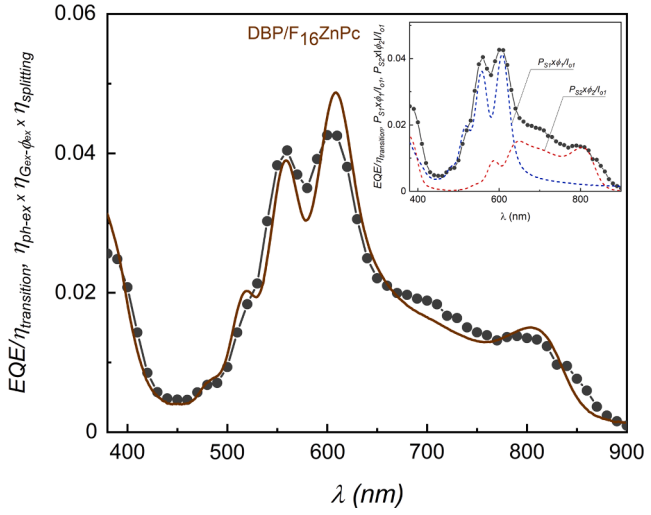

Fig. 7. Spectrum of $EQE/\eta_{transition}$ (circles) and spectrum of $\eta_{ph-ex} \times \eta_{G_{ex}-\phi_{ex}} \times \eta_{splitting}$ atL_1 = 16 nm, L_2= 10 nm, P_{S1} = 0.11 and P_{S2} = 0.12 (line) are shown in the main body of the figure. Spectra of $P_{S1}\phi_1/I_{o1}$ atL_1 = 16 nm, P_{S1} = 0.11 and $P_{S2}\phi_2/I_{o1}$ atL_2 = 10 nm, P_{S2} = 0.12 (lines) together with spectrum of $EQE/\eta_{transition}$ (circles) are shown in the inset. The curves were simulated on the basis of experimental results presented in the inset of Fig. 6.

with DBP/PTCBI is 0.91 at 608 nm and for the device with DBP/F_{16}ZnPc is 0.82 at 610 nm (see lines 1 in Fig. 3 and in Fig. 6). The comparison of ϕ_1/I_{o1} in Fig. 3 and ϕ_1/I_{o1} in Fig. 6 (see lines 2 in both figures) leads to the conclusion that the exciton flux from the DBP side in DBP/PTCBI is 30% lower than the same flux in DBP/F_{16}ZnPc in the range of strong DBP absorption.

The effect of filtering of light by DBP is easily noticed in Fig. 3 and Fig. 6. This effect causes a weak generation of excitons in EA layer within strong absorption of DBP and simultaneously causes that the flux of excitons in EA at ED/EA interface takes minima at maxima of DBP absorption. Therefore, the contribution of excitons generated in EA to the $\frac{EQE}{\eta_{transition}}$ spectrum can be only seen apart from strong DBP absorption.

On the other hand, the effect of exciton diffusion length in DBP and splitting probability of DBP excitons at ED/EA can be seen in the case of strong DBP absorption. Fig. 4 shows the spectra of $\frac{EQE}{\eta_{transition}}$ derived from

ABS of DBP layer for different sets of L_1 and P_{S1}. It was assumed that no excitons are generated in PTCBI, so $\frac{EQE}{\eta_{transition}}$ should correlate $\frac{P_{S1}\phi_1}{I_{o1}}$. As an example, spectra of $\frac{P_{S1}\phi_1}{I_{o1}}$ are shown for four sets of parameters, namely for$L_1 = 8$ nm and$P_{S1} = 1$; L_1=16 nm and$P_{S1} = 0.8$; L_1=24 nm and$P_{S1} = 0.55$; for$L_1 = 24$ nm and$P_{S1} = 1.0$. It is clearly visible that $L_1 = 8$ nm leads to too small $\frac{P_{S1}\phi_1}{I_{o1}}$ to be compared with $\frac{EQE}{\eta_{transition}}$. In order to get values corresponding to J_{sc} in the range of strong absorption of DBP the DBP exciton diffusion length should be equal to or greater than 13.8 nm. The value of $L_1 = 13.8$ nm would lead to a correlation between $\frac{P_{S1}\phi_1}{I_{o1}}$ and $\frac{EQE}{\eta_{transition}}$ under assumption that all the excitons reaching the ED/EA interface from the DBP side are effectively split into electron-hole pairs, i. e. at$P_{S1} = 1$.

In the case when $P_{S1} < 1$, the value of L_1 should be suitably greater than 13.8 nm. However, with the increase in exciton diffusion length, the structure of $P_{S1}\phi_1/I_{o1}$ becomes more expressive, i. e. the difference between local maxima and local minima of $\frac{P_{S1}\phi_1}{I_{o1}}$ increases and this effect should be also noticeable in the $EQE/\eta_{transition}$ spectrum (compare spectrum of $\frac{P_{S1}\phi_1}{I_{o1}}$ at 16 nm and 0.8 with spectrum of $\frac{P_{S1}\phi_1}{I_{o1}}$ at 24 nm and 0.55). Diffusion length for excitons in DBP is reported as equal to 16 nm [24]. For such a value of L_1, the spectrum of $\frac{P_{S1}\phi_1}{I_{o1}}$ best fitted to $EQE/\eta_{transition}$ in the strong DBP abosrption is obtained at $P_{S1} = 0.8$ (compare line 2 with circles in Fig. 4). Therefore, we can conclude that probability that excitons generated in DBP and reaching the ED/EA interface split into electron-hole pairs at DBP/PTCBI interface equals 80%.

The best fitted spectrum of $\eta_{ph-ex} \times \eta_{G_{ex}-\phi_{ex}} \times \eta_{splitting}$ encluding also exciton generated in PTCBI is presented in the main body of Fig. 5. Respecting exciton generation in PTCBI (of diffusion length equal to 9 nm and assuming splitting probability for these excitons at 0.8) the range of good correlation between $\eta_{ph-ex} \times \eta_{G_{ex}-\phi_{ex}} \times \eta_{splitting}$ and $EQE/\eta_{transition}$ becomes explicitly wider due to better fit on the left part of strong DBP absorption. Spectra of $\eta_{ph-ex} \times \eta_{G_{ex}-\phi_{ex}} \times \eta_{splitting}$ and $EQE/\eta_{transition}$ correlate well in a wide range of VIS reaching up to 650 nm. Therefore, we can say that the probability of exciton splitting at the DBP/PTCBI interface equal to 0.8 is well supported by experimental results.

However, for wavelengths longer than the wavelengths in strong DBP absorption, i.e. for wavelengths greater than ca. 650 nm, spectrum of $\eta_{ph-ex} \times \eta_{G_{ex}-\phi_{ex}} \times \eta_{splitting}$ poorly correlates with $EQE/\eta_{transition}$. Assuming an exciton splitting of 0.24 would lead to better correlation. However, the thesis about weaker dissociation of excitons generated in this range raises some doubts, therefore this problem requires further research. In general, it can be said that for relatively low *EQE* values and when the *EQE* spectrum does not give a distinct structure, there is a wide range of possibility to fit $\eta_{ph-ex} \times \eta_{G_{ex}-\phi_{ex}} \times \eta_{splitting}$ to $EQE/\eta_{transition}$ for many values of exciton diffusion length and exciton-splitting probability.

Fig. 6 shows spectrum of $EQE/\eta_{transition}$ obtained on ITO/MoO_3/DBP/F_{16}ZnPc/BCP/Ag and the spectrum of $\eta_{ph-ex} \times \eta_{G_{ex}-\phi_{ex}} \times \eta_{splitting}$ calculated from the *ABS* spectra of the DBP and F_{16}ZnPc layers. The same value as in the ITO/MoO_3/DBP/PTCBI/BCP/Ag system was taken for L_1, i.e. 16 nm. This approach is dictated not only by the same kind of material but by the same deposition conditions and the same substrates as well. To obtain the correlation between $\eta_{ph-ex} \times \eta_{G_{ex}-\phi_{ex}} \times \eta_{splitting}$ and $EQE/\eta_{transition}$ within strong DBP absorption and with$L_1 = 16$ nm we must assume P_{S1} equal to 0.11 (inset in Fig. 7). Such a value of P_{S1} compared to the value of 0.8 obtained for the ITO/MoO_3/DBP/PTCBI/DBP/Ag system clearly indicates that the excitons generated in DBP undergo much weaker splitting into electron-hole pairs at the DBP/F_{16}ZnPc interface than at the DBP/PTCBI interface.

Also the excitons generated in F_{16}ZnPc show weak splitting at the DBP/F_{16}ZnPc interface. For calculation it was assumed that$P_{S2} = 0.12$. As shown in Fig. 7, the taken values of P_{S1} and P_{S2} give a good fit of $\eta_{ph-ex} \times \eta_{G_{ex}-\phi_{ex}} \times \eta_{splitting}$ to $EQE/\eta_{transition}$ in the whole range of the studied spectrum of J_{sc}, i. e. in strong absorption of DBP and in strong absorption of F_{16}ZnPc. Regarding the fit shown (see Fig. 7) and considering$P_{S2} = 0.12$ the exciton diffusion length in F_{16}ZnPc can be estimated at 10 nm.

Summaring up, it can be concluded that our analysis clearly indicates a much higher efficiency of exciton splitting at DBP/PTCBI than at DBP/F_{16}ZnPc. The probability of exciton splitting at the DBP/PTCBI interface equal to 0.8 makes the junction quite attractive for organic photovoltaics (here also for indoor photovoltaics) and for organic photodetectors for VIS range. On the other hand, the DBP/F_{16}ZnPc interface does not show any favourable properties for photovoltaics.

5. Summary

The work presents a procedure for estimating the efficiency of exciton splitting at ED/EA interface. The procedure consists in correlating the spectrum of $\eta_{ph-ex} \times \eta_{G_{ex}-\phi_{ex}} \times \eta_{splitting}$ (obtained from the *ABS* spectra, exciton diffusion length and active layers thickness) with the spectrum of $EQE/\eta_{transition}$ (obtained from the J_{sc} spectrum at the constant density of the photon flux entering the outer active organic layer). The fitting parameters are the exciton splitting probabilities at ED/EA interface.

The presented procedure was applied to two different photovoltaic systems: ITO/MoO_3/DBP/PTCBI/BCP/Ag and ITO/MoO_3/DBP/F_{16}ZnPc/BCP/Ag. When we assume that the exciton diffusion length in DBP is unknown, we can conclude from our analysis that the exciton diffusion length in DBP is not shorter than 13.8 nm. On the other hand, if we take the value of this parameter from literature, i.e. 16 nm [24], we can conclude that probability of splitting of excitons generated in DBP equals 0.8 for DBP/PTCBI and only 0.11 for DBP/F_{16}ZnPc. Thus, instead of similarity of the energy diagrams of the two junctions, they show a distinctly different dissociation ability of excitons. Only the DBP/PTCBI interface can be considered attractive for organic photvoltaics and organic photodetection.

Declaration of Competing Interest

The authors declare that they have no known competing financial interests or personal relationships that could have appeared to influence the work reported in this paper.

References

[1] T. Kirchartz, K. Taretto, U. Rau, Efficiency Limits of Organic Bulk Heterojunction Solar Cells, J. Chem. Phys. C 113 (41) (2009) 17958–17966, https://doi.org/10.1021/jp906292h.
[2] N.C. Giebink, G.P. Wiederrecht, M.R. Wasilewski, S.R. Forrest, Thermodynamic efficiency limit of excitonic solar cells, Phys. Rev. B: Condens. Matter 83 (2011), 195326, https://doi.org/10.1103/PhysRevB.83.195326.
[3] K. Seki, A. Furube, Y. Yoshida, Theoretical limit of power conversion efficiency for organic and hybrid halide perovskite photovoltaics, Japn. J. Appl. Phys. 54 (8S1) (2015) 08KF04, https://doi.org/10.7567/JJAP.54.08KF04.
[4] G. Jarosz, M. Franz, R. Marczyński, R. Signerski, Efficiency limit of excitonic photovoltaic cells under phosphor-based white LED illumination, Org. Electron. 88 (2021) 105999, https://doi.org/10.1016/j.orgel.2020.105999.
[5] M. Gruber, J. Wagner, K. Klein, U. Hörmann, A. Opitz, M. Stutzmann, W. Brütting, Thermodynamic Efficiency Limit of Molecular Donor-acceptor Solar Cells and its Application to Diindenoperylene/C_{60}-Based Planar Heterojunction Devices, Adv. Eng. Mater. 2 (9) (2012) 1100–1108, https://doi.org/10.1002/aenm.201200077.
[6] R.A.J. Janssen, J. Nelson, Factors Limiting Device Efficiency in Organic Photovoltaics, Adv. Mater. 25 (13) (2013) 1847–1858, https://doi.org/10.1002/adma.201202873.
[7] P. Peumans, A. Yakimov, S.R. Forrest, Small molecular weight organic thin-film photodetectors and solar cells, J. Appl. Phys. 93 (7) (2003) 3693–3723, https://doi.org/10.1063/1.1534621.
[8] A.W. Hains, Z. Liang, M.A. Woodhouse, B.A. Gregg, Molecular Semiconductors in Organic Photovoltaic Cells, Chem. Rev. 110 (11) (2010) 6689–6735, https://doi.org/10.1021/cr9002984.
[9] C.B. Nielsen, S. Holliday, H.-Y. Chen, S.J. Cryer, I. McCulloch, Non-Fullerene Electron Acceptors for Use in Organic Solar Cells, Acc. Chem. Res. 48 (11) (2015) 2803–2812, https://doi.org/10.1021/acs.accounts.5b00199.

[10] L. Benatto, K.R.d.A. Sousa, M. Koehler, Driving Force for Exciton Dissociation in Organic Solar Cells: The Influence of Donor and Acceptor Relative Orientation, J. Phys. Chem. C 124 (25) (2020) 13580–13591, https://doi.org/10.1021/acs.jpcc.0c03116.
[11] T. Fukuhara, Y. Tamai, H. Ohkita, Nongeminate charge recombination in organic photovoltaics, Sustainable, Energy Fuels 4 (9) (2020) 4321–4351, https://doi.org/10.1039/D0SE00310G.
[12] C.W. Su, C.-C. Lee, Y.-Z. Li, S.-W. Liu, Influence of Singlet and Charge-Transfer Exciton on the Open-Circuit Voltage of Rubrene/Fullerene Organic Photovoltaic Device, ACS Appl. Mater. Interfaces 8 (2016) 28757–28762, https://doi.org/10.1021/acsami.6b08363.
[13] T. Linderl, T. Zechel, M. Brendel, D.M. González, J. Müller-Buschbaum, W. Pflaum, W. Brütting, Energy Losses in small-molecular Organic Photovoltaics, Adv. Eng. Mater. 7 (2017) 1700237, https://doi.org/10.1002/aenm.201700237.
[14] L. Benatto, C. A. M. Moraes, M. de Jesus Bassi, L. Wouk, L. S. Roman, M. Koehler, Kinetic Modelling of the Electric Field Dependent Exciton Quenching at the Donor-Acceptor Interface, J. Phys. Chem. C 125 (C2021) 4436-4448. https://doi.org/10.1021/acs.jpcc.0c11458.
[15] T.M. Clarke, How to split an exciton, Nat. Energy 5 (9) (2020) 644–645, https://doi.org/10.1038/s41560-020-00689-2.
[16] L. Benatto, M. de Jesus Bassi, L.C. Wouk de Menezes, L.S. Roman, M. Koehler, Kinetic Model for Photoluminecsence Quenching by Selective Excitation of D/A blends: Implications for Charge Separation in Fullerene and Non-Fullarene Organic Solar Cells, J. Mater. Chem. C 8 (2020) 8755–8769, https://doi.org/10.1039/D0TC01077D.
[17] Y. Song, A. Schubert, X. Liu, S. Bhandari, S.R. Forrest, B.D. Dunietz, E. Geva, J. P. Ogilvie, Efficient Charge Generation via Hole Transfer in Dilute Organic Donor-Fullerene Blends, J. Phys. Chem. Lett. 11 (6) (2020) 2203–2210, https://doi.org/10.1021/acs.jpclett.0c0005810.1021/acs.jpclett.0c00058.s001.
[18] K. Beltako, N. Cavassilas, M. Lannoo, F. Michelini, Insights into the Charge Separation Dynamics in Photoexcited Molecular Junctions, J. Phys. Chem. C 123 (51) (2019) 30885–30892, https://doi.org/10.1021/acs.jpcc.9b1091110.1021/acs.jpcc.9b10911.s001.
[19] O.V. Mikhnenko, P.W.M. Blom, T.-Q. Nguyen, Exciton diffusion in organic semiconductors, Energy Environ. Sci. 8 (7) (2015) 1867–1888, https://doi.org/10.1039/C5EE00925A.
[20] H.B. Naveed, K.e. Zhou, W. Ma, Interfacial and Bulk Nanostructures Control Loss of Charges in Organic Solar Cells, Acc. Chem. Res. 52 (10) (2019) 2904–2915, https://doi.org/10.1021/acs.accounts.9b00331.
[21] M. Mainville, M. Leclerc, Recent Progress on Indoor Organic Photovoltaics: From molecular Design to Production Scale, ACS Energy Lett. 5 (4) (2020) 1186–1197, https://doi.org/10.1021/acsenergylett.0c00177.
[22] Z. Zhang, Y. Lin, Organic Semiconductors for Vacuum-Deposited Planar Heterojunction Solar Cells, ACS Omega 5 (39) (2020) 24994–24999, https://doi.org/10.1021/acsomega.0c03868.
[23] D. Yokoyama, Z.Q. Wang, J.-Y. Pu, K. Kobayashi, J. Kido, J. Hong, High-efficiency simple planar heterojunction organic thin-film photovoltaics with horizontally oriented amorphous donors, Sol. Energy Mater. Sol. Cells 98 (2012) 472–475, https://doi.org/10.1016/j.solmat.2011.10.014.
[24] X. Xiao, J.D. Zimmerman, B.E. Lassiter, K.J. Bergemann, S.R. Forrest, A hybrid planar-mixed tetraphenyldibenzoperiflanthene/C_{70} photovoltaic cell, Appl. Phys. Lett. 102 (7) (2013) 073302, https://doi.org/10.1063/1.4793195.
[25] Y. Peng, L. Zhang, T.L. Andrew, High open-voltage, high fill factor single-junction organic solar cells, Appl. Phys. Lett. 105 (2014), 083304, https://doi.org/10.1063/1.4894089.
[26] T. Zhuang, T. Sano, J. Kido, Efficient small molecule-based bulk heterojunction photovoltaic cells with reduced exciton quenching in fullerene, Org. Electron. 26 (2015) 415–419, https://doi.org/10.1016/j.orgel.2015.08.015.
[27] D. Fujishima, H. Kanno, T. Kinoshita, E. Maruyama, M. Tanaka, M. Shirakawa, K. Shibata, Organic thin-film solar cel employing a novel electron-donor material, Sol. Energy Mater. Sol. Cells 93 (2009) 1029–1032, https://doi.org/10.1016/j.solmat.2008.11.034.
[28] M. Barr, C. Carbonera, R. Po, V. Bulović, K. Gleason, Cathode buffer layers based on vacuum and solution deposited poly(3,4-ethylenedioxythiphene) for efficient inverted organic solar cells, Appl. Phys. Lett. 100 (2012), 183301, https://doi.org/10.1063/1.4709481.
[29] J. Szostak, R. Signerski, J. Godlewski, Photoelectric properties of a novel MEH-PPV/F16ZnPc, Phys. Status Solidi A 210 (2013) 2353–2358, https://doi.org/10.1002/pssa.201329344.
[30] I.G. Hill, J. Schwartz, A. Kahn, Metal-Dependent charge transfer and chemical interaction at interfaces between 3,4,9,10-perylenetetracarboxylic bisimidazole and gold, silver and magnesium, Org. Electron. 1 (1) (2000) 5–13, https://doi.org/10.1016/S1566-1199(00)00002-1.
[31] C. Howells, S. Saylan, H. Kim, K. Marbou, T. Aoyama, A. Nakao, M. Uchiyama, I.D. W. Samuel, D.-W. Kim, M.S. Dahlem, P. André, Influence of Perluorinated Ionomer in PEDOT:PSS on the Rectification and degradation of organic photovoltaic cells, J. Mater. Chem A 6 (2018) 16012–16028, https://doi.org/10.1039/C8TA04098B.
[32] K.H. Park, Y. An, S. Jung, H. Park, C. Yang, The Use of an n-Type Macromolecular Additive as a Simple Yet Effective Tool for Improving and Stabilizing the Performance of Organic Solar Cells, Engergy, Environ. Sci. 9 (11) (2016) 3464–3471, https://doi.org/10.1039/C6EE02255C.
[33] M. Pfeiffer, K. Leo, N. Karl, Fermi level determination in organic thin films by the Kelvin probe method, J. Appl. Phys. 80 (12) (1996) 6880–6883, https://doi.org/10.1063/1.363757.
[34] P. Peumans, V. Bulović, S.R. Forrest, Efficient photon harvesting at high optical intensities in ultrathin organic double-heterostructure photovoltaic diodes, J. Appl. Phys. 76 (19) (2000) 2650–2652, https://doi.org/10.1063/1.126433.
[35] A. Kahn, N. Koch, W. Gao, Electronic Structure and Electrical Properties of Interfaces Between Metal and π-Conjugated Molecular Films, J. Polym. Sci., Part B: Polym. Phys. (2003) 2529–2548, https://doi.org/10.1002/polb.10642.
[36] H. Lee, S.W. Cho, Y. Yi, Interfacial electronic structure for high performance organic devices, Curr. Appl. Phys. 16 (12) (2016) 1533–1549, https://doi.org/10.1016/j.cap.2016.09.009.
[37] S. Sachdeva, J. Kaur, K. Sharma, S.K. Tripathi, Performance improvements of organic solar cell using dual cathode buffer, Curr. Appl. Phys. 18 (2018) 1592–1599, https://doi.org/10.1016/j.cap.2018.10.009.
[38] R. Marczyński, J. Szostak, R. Signerski, G. Jarosz, Electric transport in organic systems with planar DBP/F_{16}ZnPc junction on the basis of direct current and small signal admittance spectra analysis, Synth. Met. 245 (2018) 245–250, https://doi.org/10.1016/j.synthmet.2018.09.007.
[39] R. Marczyński, J. Szostak, R. Signerski, G. Jarosz, Photovoltaic effect in the single-junction DBP-PTCBI organic system under low intensity of monochromatic light, Curr. Appl. Phys. 19 (2019) 1271–1275, https://doi.org/10.1016/j.cap.2019.08.011.